Low-Loss and Broadband Nonvolatile Phase-Change Directional Coupler Switches

Peipeng Xu,*,†,‡,§ Jiajiu Zheng,†,‡ Jonathan K. Doylend,∥ and Arka Majumdar*,‡,⊥

‡Department of Electrical and Computer Engineering, University of Washington, Seattle, Washington 98195, United States
§Laboratory of Infrared Materials and Devices, Advanced Technology Research Institute, Ningbo University, Ningbo 315211, China
∥Silicon Photonic Products Division, Intel Corporation, Santa Clara, California 95054, United States
⊥Department of Physics, University of Washington, Seattle, Washington 98195, United States

🅢 Supporting Information

ABSTRACT: An optical equivalent of the field-programmable gate array (FPGA) is of great interest to large-scale photonic integrated circuits. Previous programmable photonic devices relying on the weak, volatile thermo-optic or electro-optic effect usually suffer from a large footprint and high energy consumption. Phase change materials (PCMs) offer a promising solution due to the large nonvolatile change in the refractive index upon phase transition. However, the large optical loss in PCMs poses a serious problem. Here, by exploiting an asymmetric directional coupler design, we demonstrate nonvolatile PCM-clad silicon photonic 1 × 2 and 2 × 2 switches with a low insertion loss of ∼1 dB and a compact coupling length of ∼30 μm while maintaining a small crosstalk less than −10 dB over a bandwidth of 30 nm. The reported optical switches will function as the building blocks of the meshes in the optical FPGAs for applications such as optical interconnects, neuromorphic computing, quantum computing, and microwave photonics.

KEYWORDS: phase-change materials, silicon photonics, integrated photonic devices, nonvolatile, reconfigurable photonics, optical switches
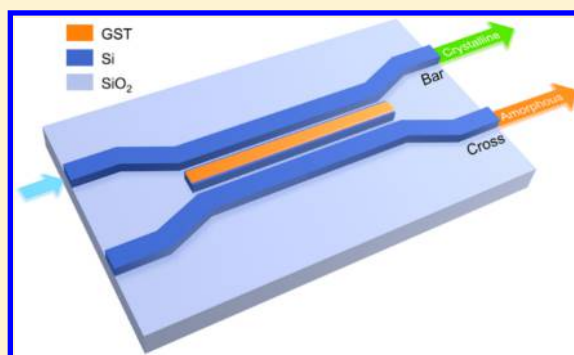
T remendous progress has been made in photonic integrated circuits (PICs) over the last two decades, revealing their potential to create photonic systems with small footprints, low power consumption, high-speed operation, and low-cost packaging. With PICs going fabless,[1] large-scale PICs have recently been reported, enabling systems with complexities far beyond classical benchtop optics.[2−4] Many of these PICs rely on programmable and generic photonic circuits[5−8] analogous to the field-programmable gate arrays (FPGAs) in electronics. Contrary to the scheme of application-specific PICs, where specific circuit architectures are designed to implement particular functions, such programmable PICs bring about far greater flexibility and effective cost reduction and thus will be a promising approach to realize applications such as routing fabrics in optical communication networks, reconfigurable logic gates in optical information processing, and multifunctional lab on a chip in optical sensing.[6]

Programmable optical cores employing a grid of Mach−Zehnder (MZ) switches have been demonstrated by several groups.[5,7,8] In these works, the on-chip optical switches can be reconfigured to the cross or bar state, forming one of the most fundamental and critical components in programmable PICs. Current optical switches in PICs, however, primarily rely on the weak modulation of the refractive index (usually Δn <

0.01) from the free-carrier dispersion[9,10] or thermo-optic[11] effects, resulting in a large footprint (several hundred micrometers) and high power consumption (typically several milliwatts). Resonator-based switches can help improve the modulation strength[12] but suffer from intrinsic narrow optical bandwidth as well as high sensitivity to fabrication imperfections and temperature fluctuations.[13] Moreover, as the switching mechanism is volatile, a constant power supply is required to maintain the switched state.

To overcome these fundamental limitations, phase-change materials (PCMs) have been proposed to provide strong modulation and nonvolatility for on-chip tunable optical devices[14,15] due to several unique properties: phase transition between amorphous and crystalline states with considerable modulation in electrical resistivity and optical constants (Δn > 1) over a broad spectral region,[16] state retention for years in no need of extra power,[17] fast and reversible switching of the states with nanosecond optical or electrical pulses,[18,19] high endurance up to 10^{15} switching cycles,[20] and excellent scalability.[21] Therefore, PCMs have emerged for a plethora of PIC applications such as optical switches,[15,22−28] optical
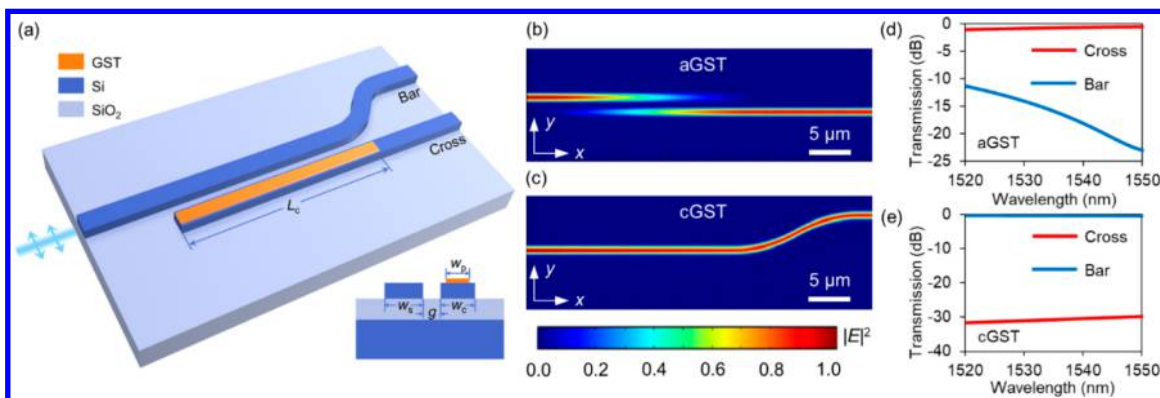
A

Figure 1. Design of the 1 × 2 DC switch. (a) Schematic of the switch. (b, c) Normalized optical field intensity distribution of the switch for (b) aGST and (c) cGST simulated by the 3D finite-difference time-domain method (Lumerical) at 1550 nm. (d, e) Calculated transmission spectra at the cross and bar ports for (d) aGST and (e) cGST.

modulators,[25,29] photonic memories,[30,31] and optical computing.[32,33]

Practical applications of programmable PICs require optical switches to have a multiport and broadband characteristic. Current experimental demonstrations of PCM-integrated switches, however, are either single-port[22,24,27] or narrowband.[15,23,26] PCM-integrated MZ switches can afford broadband operation.[11] Unfortunately, their performance including the crosstalk (CT, defined as the contrast ratio between the two output ports) and insertion loss (IL) is dramatically sacrificed due to the large absorptive loss from crystalline PCMs.

Here, we demonstrate compact (~30 μm), low-loss (~1 dB), and broadband (over 30 nm with CT < −10 dB) 1 × 2 and 2 × 2 switches using the PCM, $Ge_2Sb_2Te_5$ (GST), based on the previously built nonvolatile programmable GST-on-silicon platform[15] and the asymmetric directional coupler (DC) switch design,[28,34] bypassing the high loss associated with the crystalline state.

RESULTS AND DISCUSSION

Figure 1a shows the schematic of the 1 × 2 DC switch. The asymmetric coupling region consists of a normal silicon strip waveguide (SW) and a GST-on-silicon hybrid waveguide (HW) where a thin layer of GST is placed on silicon. When the GST is in the low-loss amorphous state, the optimized structure of the silicon SW and the HW can meet the phase-matching condition for TE polarization, leading to the cross state of the switch with a low IL (Figure 1b). Once the GST is transformed to the lossy crystalline state, the phase-matching condition is significantly altered due to the strong modification of the mode in the HW induced by the dramatic difference of complex refractive indices between amorphous GST (aGST) and crystalline GST (cGST) (see Supporting Information). As a result, light is diverted away from the HW forming the bar state of the switch with low attenuation ensured by minimal optical field interaction with the lossy GST layer (Figure 1c).

To determine the widths of the waveguides (w_s, w_c) appropriately, we analyze the effective indices of the eigenmodes supported in the silicon SW and the GST-on-silicon HW (see Supporting Information). The simulations are performed using the frequency-domain finite-element method (COMSOL Multiphysics). The width of the silicon SW (w_s) is chosen as 450 nm to ensure single-mode operation. The width of the GST (w_p) is set to be 100 nm smaller than the core

width of the HW (w_c), which can be easily achieved within the alignment precision of the electron-beam lithography (EBL). w_c is optimally chosen as 420 nm so that the phase-matching condition could be satisfied for aGST. Therefore, the input TE-polarized light will be evanescently coupled to the cross port completely with an appropriate coupling length. Considering the trade-off between the coupling length (L_c) and the insertion loss in the crystalline state (IL$_{cGST}$; see Supporting Information), the gap (g) between the two waveguides is chosen to be 150 nm while ensuring reliable fabrication of the coupling region. The coupling length given by $L_c = \lambda_0/2(n_{aGST1} - n_{aGST2})$ is thus calculated as compact as ~24 μm, where n_{aGST1} and n_{aGST2} are, respectively, the effective indices of the first order (even) and second order (odd) supermodes in the two-waveguide system, $\lambda_0 = 1550$ nm is the wavelength.

Figure 1d,e show the calculated transmission spectral response of the 1 × 2 DC switch in both states. When the GST is in the amorphous state, the optical switch attains a small IL < 1 dB and CT from −11 to −23 dB over the wavelength range of 1520−1550 nm. For the crystalline state, since almost no evanescent coupling occurs due to the phase mismatch, the spectral response to the input light is quite flat and broadband. The corresponding IL and CT are <0.6 dB and <−29 dB across the whole wavelength range.

The devices were fabricated (see Methods) using an SOI wafer with a 220-nm-thick silicon layer on top of a 3-μm-thick buried oxide layer. The pattern was defined via EBL and transferred to the top silicon layer by inductively coupled plasma etching. Deposition of 20 nm GST and 11 nm indium tin oxide (ITO to avoid GST oxidation) on the HWs was completed using a second EBL step followed by the sputtering and lift-off process. Figure 2a,b shows the optical microscope and scanning electron microscope (SEM) images of the fabricated 1 × 2 DC switch. A false-colored SEM image of the coupling region is shown in Figure 2c, where the GST layer is clearly resolved.

An off-chip optical fiber setup was used to measure the spectral response of the fabricated devices (see Methods). For each device, we measured the transmission right after the deposition of the GST, which is initially in the amorphous state because of the low sputtering temperature. After that, rapid thermal annealing (RTA) of the chip at 200 °C for 10 min in a N_2 atmosphere was performed to actuate the phase transition from aGST to cGST.[15] The measurement results of the 1 × 2
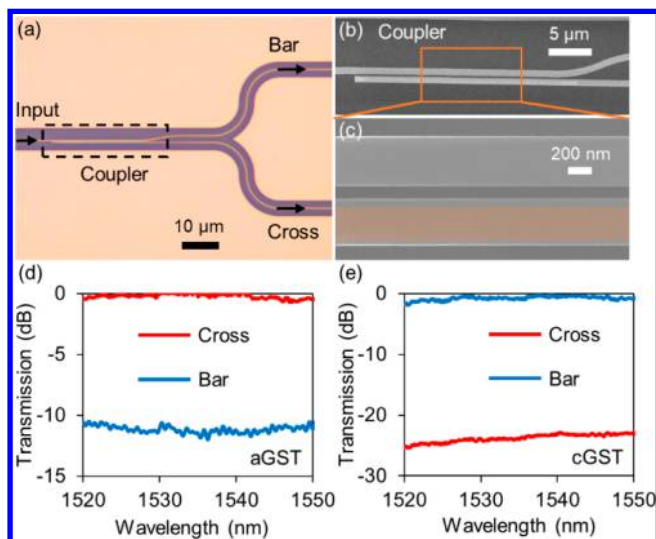
Figure 2. Experimental results of the 1×2 DC switch. (a) Optical microscope image of the fabricated switch. (b) SEM image of the switch. (c) An enlarged view of the coupling region highlighted by the orange rectangle in (b) with the GST false-colored. (d, e) Measured transmission at the cross and bar ports with the GST in the (d) amorphous and (e) crystalline states.

the light coupling mechanism by analyzing the supermodes in the coupling region (see Supporting Information). In this calculation, we adopt the same parameters used in the 1×2 switch with $w_s = 450$ nm, $g = 150$ nm, and $w_p = w_c - 100$ nm. To meet the phase-matching condition, the width of the HW (w_c) is optimally chosen as 422 nm. Once the GST is crystallized, the three-waveguide system effectively boils down to two separated SWs because of the much higher effective index of the HW. In this case, only the even and odd supermodes can be supported in the coupler. The gap between the two SWs is $w_p + 2g$, resulting in a much larger coupling length (L_{cGST}). More specifically, when $g = 150$ nm, L_{cGST} is calculated to be 516 μm while the coupling length for aGST (L_{aGST}) is 35 μm (see Supporting Information), leading to a large ratio of $L_{cGST}/L_{aGST} = 14.7$. Hence, after a specific coupling length (L_c, designed for the maximum transmission in the amorphous state, that is, L_{aGST}), the input light is almost not cross-coupled but propagates directly to the bar port as if the central HW does not exist (Figure 3c). This behavior can be further verified by the fact that the effective indices of the supermodes almost remain unchanged when w_c changes as there is no field distribution in the GST-on-silicon HW (see Supporting Information).

Figure 3d,e show the simulated spectral response of the designed 2×2 DC switch for aGST and cGST when launching the light from one of the input ports. The device exhibits low ILs of <1 dB in both states when the wavelength varies from 1510 to 1540 nm. The bandwidth for achieving a CT less than -15 dB in the amorphous state and less than -20 dB in the crystalline state is more than 25 nm, enabling broadband switching operation.

Figure 4a,b shows the microscope and SEM images of the fabricated 2×2 DC switch. A false-colored SEM image of the coupling region is shown in Figure 4c where the GST layer is clearly resolved. The measured transmission spectra of the 2×2 DC switch are shown in Figure 4d,e. For aGST, the IL was measured to be approximately 1 dB and the CT is less than ~ -15 dB at the wavelength ranging from 1510 to 1540 nm, agreeing well with the simulation results. For cGST, the IL through the switch is approximately $1-2$ dB and the CT is less than -10 dB with a bandwidth of over 30 nm. The degraded IL and CT compared with the simulation results are mainly attributed to the gap discrepancy due to the fabrication imperfection and positional deviation of the GST layer owing to the limited alignment precision.
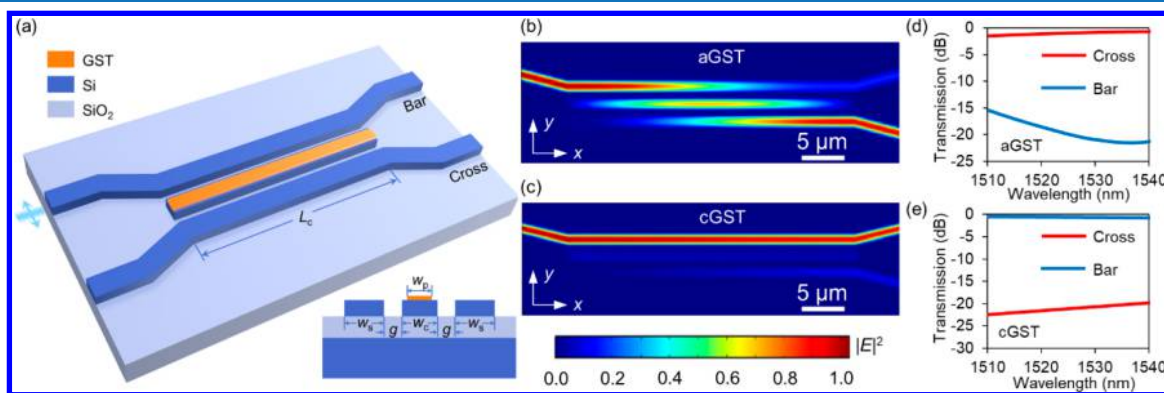
DC switch are shown in Figure 2d,e. For the wavelength range of 1520−1550 nm, the ILs were measured to be approximately 1 dB for both states and the CT was measured to be <−10 dB for aGST and <−22 dB for cGST. The discrepancy between the measured CTs and the design targets is primarily due to the fabrication-induced gap change and positional deviation of the GST layer owing to the limited alignment precision.

We extend the DC design scheme to build a 2×2 switch. Figure 3a shows the schematic diagram of the 2×2 DC switch based on the three-waveguide DC. The operating principle of the proposed switch relies on the considerable mode modification of the TE-polarized supermodes in the three-waveguide system due to the GST phase transition. When the GST is in the amorphous state, the device functions as a three-waveguide DC and the complete power transfer could be achieved when the phase-matching condition (i.e., the effective indices of the three supermodes are evenly spaced) is satisfied. Thus, the input light couples to the low-loss GST-on-silicon HW and passes through the cross port (Figure 3b). We study

Figure 3. Design of the 2×2 DC switch. (a) Schematic of the switch. (b, c) Normalized optical field intensity distribution in the device for (b) aGST and (c) cGST simulated by the 3D eigenmode expansion method (Lumerical) at 1550 nm. (d, e) Calculated transmission spectra at the cross and bar ports for (d) aGST and (e) cGST.
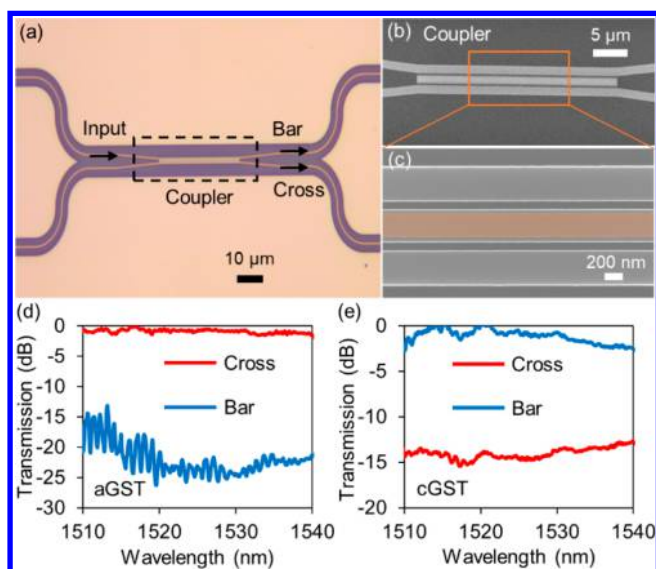
Figure 4. Experimental results of the 2 × 2 DC switch. (a) Optical microscope image of the fabricated switch. (b) SEM image of the switch. (c) An enlarged view of the coupling region highlighted by the orange rectangle in (b) with the GST false-colored. (d, e) Measured transmission at the cross and bar ports with the GST in the (d) amorphous and (e) crystalline states.

CONCLUSIONS

By exploiting the high optical contrast of PCMs and asymmetric DC design, we demonstrated compact (~30 μm) nonvolatile 1 × 2 and 2 × 2 switches with low-loss (~1 dB) and broadband (over 30 nm with CT < −10 dB) operations on the silicon photonic platform. Although the reported switches are optimized for TE polarization, similar design can be conducted for TM operation (see Supporting Information). With emerging wide-bandgap PCMs[35,36] and better fabrication, further improvement of the performance including IL and CT can be expected. The optical bandwidth of the designed switches (see Supporting Information) is primarily limited by the wavelength-dependent coupling length and phase-matching condition mainly due to the waveguide dispersion and can be further improved by utilizing the adiabatic,[37] bent,[11] or multisection[38] DC. As a proof of concept, thermal heating was employed to actuate the phase transition in this paper. For practical applications in a large-scale PIC, on-chip electrical switching using transparent conductive heaters[27] such as ITO, graphene, or silicon can be considered with the switching speed as fast as ~10 MHz,[27] which is much faster than the traditional thermo-optic switches (~100 kHz).[11] From the volume of the GST needed in the switches, the reconfiguration energy for phase transition is estimated to be ~2 nJ,[15] only an order of magnitude larger than the thermodynamic limit.[20] Note that, due to the nonvolatility of the GST, no more energy is required after switching. The availability of such on-chip nonvolatile switching technology paves the way for optical FPGAs and sheds light on their applications including optical interconnects, neuromorphic computing, quantum computing, and microwave photonics.

METHODS

Fabrication and Optical Characterization Setup. The designed on-chip optical switches were fabricated using the SOI wafer with a 220-nm-thick silicon layer on top of a 3-μm-

thick buried oxide layer. The pattern was defined by a JEOL JBX-6300FS 100 kV EBL system using a positive tone ZEP-520A resist and transferred to the silicon layer by inductively coupled plasma (ICP) etcher utilizing a gas mixture of SF_6 and C_4F_8. Next, a positive electron beam resist, PMMA was spun on the sample and a second EBL exposure was used to define the window for the GST deposition on the HWs. Finally, 20 nm GST and 11 nm indium tin oxide (ITO) were deposited using a magnetron sputtering system followed by a lift-off process. The on-chip devices were characterized by an off-chip optical fiber setup. The focusing subwavelength grating couplers[39] were fabricated at the input ports and output ports for fiber-chip coupling and polarization selectivity. The polarization of the input light was controlled to match the fundamental quasi-TE mode of the waveguide by a manual fiber polarization controller (Thorlabs FPC526). The straight single-mode waveguides with the same grating couplers were also fabricated on the same chip to normalize the spectra. A tunable continuous wave laser (Santec TSL-510) and a low-noise power meter (Keysight 81634B) were used to measure the performance of the fabricated devices.

■ ASSOCIATED CONTENT

Ⓢ Supporting Information

The Supporting Information is available free of charge on the ACS Publications website at DOI: 10.1021/acsphotonics.8b01628.

> The design of the 1 × 2 and 2 × 2 switches (sections S1 and S2); optical bandwidth of the switches (section S3); discussion of the switch design for TM polarization (section S4) (PDF)

■ AUTHOR INFORMATION

Corresponding Authors
*E-mail: xupeipeng@nbu.edu.cn.
*E-mail: arka@uw.edu.

ORCID Ⓘ
Jiajiu Zheng: 0000-0003-1527-201X
Arka Majumdar: 0000-0003-0917-590X

Author Contributions
†These authors contributed equally to this work.

Notes
The authors declare no competing financial interest.

■ ACKNOWLEDGMENTS

■ REFERENCES

(1) Hochberg, M.; Baehr-Jones, T. Towards fabless silicon photonics. *Nat. Photonics* **2010**, *4*, 492−494.

(2) Sun, C.; Wade, M. T.; Lee, Y.; Orcutt, J. S.; Alloatti, L.; Georgas, M. S.; Waterman, A. S.; Shainline, J. M.; Avizienis, R. R.; Lin, S. Single-chip microprocessor that communicates directly using light. *Nature* **2015**, *528*, 534−538.

(3) Shen, Y.; Harris, N. C.; Skirlo, S.; Prabhu, M.; Baehr-Jones, T.; Hochberg, M.; Sun, X.; Zhao, S.; Larochelle, H.; Englund, D. Deep learning with coherent nanophotonic circuits. *Nat. Photonics* **2017**, *11*, 441−446.

(4) Wang, J.; Paesani, S.; Ding, Y.; Santagati, R.; Skrzypczyk, P.; Salavrakos, A.; Tura, J.; Augusiak, R.; Mančinska, L.; Bacco, D.; Bonneau, D.; Silverstone, J. W.; Gong, Q.; Acín, A.; Rottwitt, K.; Oxenløwe, L. K.; O'Brien, J. L.; Laing, A.; Thompson, M. G. Multidimensional quantum entanglement with large-scale integrated optics. *Science* **2018**, *360*, 285−291.

(5) Zhuang, L.; Roeloffzen, C. G.; Hoekman, M.; Boller, K.-J.; Lowery, A. J. Programmable photonic signal processor chip for radiofrequency applications. *Optica* **2015**, *2*, 854−859.

(6) Graydon, O. Birth of the programmable optical chip. *Nat. Photonics* **2016**, *10*, 1.

(7) Liu, W.; Li, M.; Guzzon, R. S.; Norberg, E. J.; Parker, J. S.; Lu, M.; Coldren, L. A.; Yao, J. A fully reconfigurable photonic integrated signal processor. *Nat. Photonics* **2016**, *10*, 190−195.

(8) Pérez, D.; Gasulla, I.; Crudgington, L.; Thomson, D. J.; Khokhar, A. Z.; Li, K.; Cao, W.; Mashanovich, G. Z.; Capmany, J. Multipurpose silicon photonics signal processor core. *Nat. Commun.* **2017**, *8*, 636.

(9) Lu, L.; Zhao, S.; Zhou, L.; Li, D.; Li, Z.; Wang, M.; Li, X.; Chen, J. 16× 16 non-blocking silicon optical switch based on electro-optic Mach-Zehnder interferometers. *Opt. Express* **2016**, *24*, 9295−9307.

(10) Qiao, L.; Tang, W.; Chu, T. 32× 32 silicon electro-optic switch with built-in monitors and balanced-status units. *Sci. Rep.* **2017**, *7*, 42306.

(11) Chen, S.; Shi, Y.; He, S.; Dai, D. Low-loss and broadband 2 × 2 silicon thermo-optic Mach−Zehnder switch with bent directional couplers. *Opt. Lett.* **2016**, *41*, 836−839.

(12) Sherwood-Droz, N.; Wang, H.; Chen, L.; Lee, B. G.; Biberman, A.; Bergman, K.; Lipson, M. Optical 4 × 4 hitless silicon router for optical Networks-on-Chip (NoC). *Opt. Express* **2008**, *16*, 15915−15922.

(13) Reed, G. T.; Mashanovich, G.; Gardes, F. Y.; Thomson, D. J. Silicon optical modulators. *Nat. Photonics* **2010**, *4*, 518−526.

(14) Wuttig, M.; Bhaskaran, H.; Taubner, T. Phase-change materials for non-volatile photonic applications. *Nat. Photonics* **2017**, *11*, 465−476.

(15) Zheng, J.; Khanolkar, A.; Xu, P.; Colburn, S.; Deshmukh, S.; Myers, J.; Frantz, J.; Pop, E.; Hendrickson, J.; Doylend, J. GST-on-silicon hybrid nanophotonic integrated circuits: a non-volatile quasi-continuously reprogrammable platform. *Opt. Mater. Express* **2018**, *8*, 1551−1561.

(16) Shportko, K.; Kremers, S.; Woda, M.; Lencer, D.; Robertson, J.; Wuttig, M. Resonant bonding in crystalline phase-change materials. *Nat. Mater.* **2008**, *7*, 653−658.

(17) Wuttig, M.; Yamada, N. Phase-change materials for rewriteable data storage. *Nat. Mater.* **2007**, *6*, 824.

(18) Wutting, R. *Phase Change Materials: Science and Applications*; Springer: New York, NY, U.S.A., 2009.

(19) Loke, D.; Lee, T.; Wang, W.; Shi, L.; Zhao, R.; Yeo, Y.; Chong, T.; Elliott, S. Breaking the speed limits of phase-change memory. *Science* **2012**, *336*, 1566−1569.

(20) Raoux, S.; Xiong, F.; Wuttig, M.; Pop, E. Phase change materials and phase change memory. *MRS Bull.* **2014**, *39*, 703−710.

(21) Raoux, S.; Burr, G. W.; Breitwisch, M. J.; Rettner, C. T.; Chen, Y.-C.; Shelby, R. M.; Salinga, M.; Krebs, D.; Chen, S.-H.; Lung, H.-L. Phase-change random access memory: A scalable technology. *IBM J. Res. Dev.* **2008**, *52*, 465−479.

(22) Tanaka, D.; Shoji, Y.; Kuwahara, M.; Wang, X.; Kintaka, K.; Kawashima, H.; Toyosaki, T.; Ikuma, Y.; Tsuda, H. Ultra-small, self-holding, optical gate switch using $Ge_2Sb_2Te_5$ with a multi-mode Si waveguide. *Opt. Express* **2012**, *20*, 10283−10294.

(23) Rudé, M.; Pello, J.; Simpson, R. E.; Osmond, J.; Roelkens, G.; van der Tol, J. J.; Pruneri, V. Optical switching at 1.55 μm in silicon racetrack resonators using phase change materials. *Appl. Phys. Lett.* **2013**, *103*, 141119.

(24) Moriyama, T.; Tanaka, D.; Jain, P.; Kawashima, H.; Kuwahara, M.; Wang, X.; Tsuda, H. Ultra-compact, self-holding asymmetric Mach-Zehnder interferometer switch using Ge2Sb2Te5 phase-change material. *IEICE Electronics Express* **2014**, *11*, 20140538−20140538.

(25) Liang, H.; Soref, R.; Mu, J.; Majumdar, A.; Li, X.; Huang, W.-P. Simulations of Silicon-on-Insulator Channel-Waveguide Electro-optical 2 × 2 Switches and 1 × 1 Modulators Using a $Ge_2Sb_2Te_5$ Self-Holding Layer. *J. Lightwave Technol.* **2015**, *33*, 1805−1813.

(26) Stegmaier, M.; Ríos, C.; Bhaskaran, H.; Wright, C. D.; Pernice, W. H. Nonvolatile All-Optical 1× 2 Switch for Chipscale Photonic Networks. *Adv. Opt. Mater.* **2017**, *5*, 1600346.

(27) Kentaro, K.; Masashi, K.; Hitoshi, K.; Tohru, T.; Hiroyuki, T. Current-driven phase-change optical gate switch using indium−tin-oxide heater. *Appl. Phys. Express* **2017**, *10*, No. 072201.

(28) Zhang, Q.; Zhang, Y.; Li, J.; Soref, R.; Gu, T.; Hu, J. Broadband nonvolatile photonic switching based on optical phase change materials: beyond the classical figure-of-merit. *Opt. Lett.* **2018**, *43*, 94−97.

(29) Yu, Z.; Zheng, J.; Xu, P.; Zhang, W.; Wu, Y. Ultracompact Electro-Optical Modulator-Based Ge2Sb2Te5 on Silicon. *IEEE Photonics Technol. Lett.* **2018**, *30*, 250−253.

(30) Rios, C.; Hosseini, P.; Wright, C. D.; Bhaskaran, H.; Pernice, W. H. P. On-Chip Photonic Memory Elements Employing Phase-Change Materials. *Adv. Mater.* **2014**, *26*, 1372−1377.

(31) Ríos, C.; Stegmaier, M.; Hosseini, P.; Wang, D.; Scherer, T.; Wright, C. D.; Bhaskaran, H.; Pernice, W. H. Integrated all-photonic non-volatile multi-level memory. *Nat. Photonics* **2015**, *9*, 725−732.

(32) Feldmann, J.; Stegmaier, M.; Gruhler, N.; Ríos, C.; Bhaskaran, H.; Wright, C.; Pernice, W. Calculating with light using a chip-scale all-optical abacus. *Nat. Commun.* **2017**, *8*, 1256.

(33) Cheng, Z.; Ríos, C.; Pernice, W. H. P.; Wright, C. D.; Bhaskaran, H. On-chip photonic synapse. *Science Advances* **2017**, *3*, No. e1700160.

(34) Soref, R. Tutorial: Integrated-photonic switching structures. *APL Photon.* **2018**, *3*, No. 021101.

(35) Zhang, Y.; Chou, J. B.; Li, J.; Li, H.; Du, Q.; Yadav, A.; Zhou, S.; Shalaginov, M. Y.; Fang, Z.; Zhong, H. Extreme Broadband Transparent Optical Phase Change Materials for High-Performance Nonvolatile Photonics. *arXiv; preprint arXiv:1811.00526* **2018**, na.

(36) Dong, W.; Liu, H.; Behera, J. K.; Lu, L.; Ng, R. J.; Sreekanth, K. V.; Zhou, X.; Yang, J. K.; Simpson, R. E. Wide Bandgap Phase Change Material Tuned Visible Photonics. *Adv. Funct. Mater.* **2018**, *1806181*.

(37) Yun, H.; Shi, W.; Wang, Y.; Chrostowski, L.; Jaeger, N. A. F. In 2 × 2 adiabatic 3-dB coupler on silicon-on-insulator rib waveguides, Photonics North 2013. *Proc. SPIE* **2013**, 6.

(38) Lu, Z. Q.; Yun, H.; Wang, Y.; Chen, Z. T.; Zhang, F.; Jaeger, N. A. F.; Chrostowski, L. Broadband silicon photonic directional coupler using asymmetric-waveguide based phase control. *Opt. Express* **2015**, *23* (3), 3795−3806.

(39) Wang, Y.; Wang, X.; Flueckiger, J.; Yun, H.; Shi, W.; Bojko, R.; Jaeger, N. A.; Chrostowski, L. Focusing sub-wavelength grating couplers with low back reflections for rapid prototyping of silicon photonic circuits. *Opt. Express* **2014**, *22*, 20652−20662.